Available online at BCREC website: https://bcrec.id

Bulletin of Chemical Reaction Engineering & Catalysis, 17 (2) 2022, 286-303

Research Article

Green Synthesis, Characterization, and Catalytic Activity of Amine-multiwalled Carbon Nanotube for Biodiesel Production

Maria Cristina Macawile[1,3,4,*], Alva Durian[1,3], Rugi Vicente Rubi[1], Armando Quitain[1,2], Tetsuya Kida[1], Raymond Tan[3], Luis Razon[3], Joseph Auresenia[3]

[1]*Faculty of Advanced Science and Technology, Kumamoto University, 2-40-1 Kurokami, Chuo-ku, Kumamoto 860-8555 Japan.*
[2]*College of Cross-Cultural and Multidisciplinary Studies, Kumamoto University, 2-40-1 Kurokami, Chuo-ku, Kumamoto 860-8555 Japan.*
[3]*Chemical Engineering Department, Gokongwei College of Engineering, De La Salle University-Manila, 2401 Taft Avenue, Malate, Manila 1004 Philippines.*
[4]*College of Engineering, Architecture and Technology, De La Salle University Dasmarinas, Cavite DBB-B, 4115 West Ave, Dasmariñas, Cavite 4114 Philippines.*

Received: 13th January 2022; Revised: 26th February 2022; Accepted: 28th February 2022
Available online: 9th March 2022; Published regularly: June 2022

Abstract

An amine-functionalized multiwalled carbon nanotube (MWCNT) was prepared for use as a basic heterogeneous catalyst for the conversion of *Cocos nucifera* (coconut) oil and *Hibiscus cannabinus* (kenaf) oil to biodiesel. The 3-aminopropyltrimethoxysilane (3-APTMS) was chosen to form an amine-reactive surface to bind with hydroxyl (−OH) and carboxyl (−COOH) groups of oxidized MWCNT. Silanization took place using a green surface modification method in which supercritical carbon dioxide fluid was utilized under the following conditions: 55 °C, 9 MPa, and 1 h. The synthesized catalyst was characterized using Thermogravimetric analysis (TGA), Fourier transform infrared (FTIR), Field emission scanning electron microscopy–energy dispersive x-ray (FESEM-EDX), Time-of-flight secondary ion mass spectrometry (TOF-SIMS), X-ray powder diffraction (XRD), and Brunauer–Emmett-Teller (BET). Transesterification of coconut oil using 10 wt% NH_2-MWCNT catalyst (3 wt% APTMS), 12:1 molar ratio of methanol and oil at 63 °C for 1 h resulted in a >95% conversion. On the other hand, the same catalyst was used in the transesterification of kenaf oil, and formation of ammonium carboxylated salt was observed. The effects of temperature, pressure, and silane concentration on surface modification of MWCNT were evaluated in terms of the catalyst's basic site density and fatty acid methyl ester conversion. The results indicate that reaction temperature and silane concentration had the most significant effects.

Keywords: Amine; Aminosilane; Biodiesel; Supercritical carbon dioxide; Transesterification

How to Cite: M.C. Macawile, A. Durian, R.V. Rubi, A. Quitain, T. Kida, R. Tan, L. Razon, J. Auresenia (2022). Green Synthesis, Characterization, and Catalytic Activity of Amine-multiwalled Carbon Nanotube for Biodiesel Production. *Bulletin of Chemical Reaction Engineering & Catalysis*, 17(2), 286-303 (doi:10.9767/bcrec.17.2.13402.286-303)

Permalink/DOI: https://doi.org/10.9767/bcrec.17.2.13402.286-303

1. Introduction

The global energy demand has grown exponentially, and the continued use of non-renewable energy sources like coal, oil, and natural gas has resulted in their gradual depletion [1]. One alternative solution that has long been studied to address this issue is the production and use of biofuel. Biodiesel, a liquid biofuel, is a promising alternative for a diesel engine or

* Corresponding Author.
Email: mamacawile@dlsud.edu.ph; macawile.cris@gmail.com (M.C. Macawile); Tel: +63-046-4811900 loc.3074

petrodiesel. Over the past decades, it became well-known for its biodegradability, renewability, lower exhaust emissions, higher flashpoint for easier handling, and lubricity. Consequently, numerous studies are carried out to improve its quality, consistency, and long-term viability [2–4].

Transesterification is an equilibrium reaction describing the alcoholysis of carboxylic esters carried out in the presence of an acid or base catalyst to produce fatty acid methyl esters [5]. A heterogeneous base catalyst is often used in the transesterification of low free fatty acid oil and offers a more environmentally desirable option for producing biodiesel [6]. These solid base catalysts are reusable, regenerative, and less corrosive, leading to safer and more environmentally friendly operations. Some of the recently discovered solid base catalysts for biodiesel production are hydrotalcite, oxides of metal (*e.g.*, CaO, MgO, or SrO), oxides of alkali-doped metal oxides (*e.g.*, MgO/Al_2O_3, CaO/Al_2O_3, Li/CaO), oxides of mixed metal (*e.g.*, Ca/Mg, Ca/Zn), alkali metal oxides (*e.g.*, Na/NaOH/γ-Al_2O_3, K_2CO_3/Al_2O_3 reinforced on Al_2O_3) and magnetic composites [7–9].

In addition to many other novel base catalysts produced, an amine catalyst has also gained acceptance in homogeneous and heterogeneous transesterification of oils [10,11]. Amine, classified as a weak-base, has a lone pair of electrons on its nitrogen atom that can accept protons, such as H^+ and function as a Bronsted-Lowry base in a chemical reaction. Despite being classified as a weak base, it has shown a unique basicity strength which can be determined by measuring its logarithmic base dissociation constant (pK_b) value. Primary amines have the lowest pK_b values indicating a stronger base property than secondary and tertiary amines.

Amino-organosilane is one of the most commonly used primary amines, and 3-aminopropyltriethoxysilane and 3-aminopropyltrimethoxysilane are examples of this chemical compound. Organosilane, an inexpensive coupling agent, is generally used as a surface modifier, primer, or adhesive [12]. Some of its other applications are in CO_2 adsorption [13,14], heavy metal detection [15], interface reagent adhesion [16], synthesis of ethyl acetate [17], manufacturing of epoxy coatings for corrosion protection [18], anti-fouling thin-film composite [19], and base catalyst for biodiesel production [20].

Studies that used aminosilane catalysts in biodiesel production are also found in the references [21,22]. Although significant results have been recorded, environmental harmful effects may occur during the catalyst production as a result of using toxic solvents, longer reaction time, and inclusion of more chemicals. To minimize environmental impacts from these activities, the use of fluids (*e.g.*, water or CO_2) in their supercritical states is examined and utilized in the field of green chemical processes. Presently, there are only a few discussions on the catalytic activity of a heterogeneous base catalyst synthesized with aminosilane and MWCNT under supercritical CO_2 conditions for biodiesel production. Supercritical carbon dioxide (T_c = 31.10 °C; P_c = 7.39 MPa) is an inert, inexpensive, clean fluid, and a promising alternative to toxic volatile organic compounds such as toluene [23]. It also has zero surface tension, which effectively improves nanomaterial surface wetting, enabling chemical reaction, and surface modification [24]. Based on our previous research work, oxidized mercaptosilane was successfully grafted on MWCNT using $scCO_2$, and a high free fatty acid oil was successfully catalyzed [25].

This study focuses on $scCO_2$ grafting of a primary amine on MWCNT and its catalytic activity in converting two types of oil with substantially different acid values. The effects of temperature, pressure and silane concentration on the amount of amine grafted on the surface and its influence on biodiesel conversion are also presented. This research is a result of our extensive efforts to develop high-performance green catalysts using organosilane compounds.

2. Materials and Methods

2.1 Material

A pristine MWCNT (p-MWCNT) with a length of 10–30 mm and diameter of 20–30 nm was purchased from Chengdu Organic Chemicals Co., Ltd (China). The chemicals used in oxidation of p-MWCNT, such as hydrochloric acid (HCl, 36%) and nitric acid (HNO_3, 70%), were procured from Wako Pure Chemical Industries (Japan). The chemicals used in surface modification, specifically 3-aminopropyltrimethoxysilane (3-APTMS, 98%) and carbon dioxide (CO_2, 99.9% purity), were supplied by Wako Pure Chemical Industries (Japan) and Uchimura Sanso Co., Ltd (Japan), respectively. Inorganic chemicals such as boron trifluoride in methanol complex solution (49%–53% BF_3, Tokyo Chemical Industry Co., Ltd), sodium chloride (NaCl, Wako Pure Chemical Industries), sodium sulfate (Na_2SO_4, Wako Pure Chemical Industries), potassium hydro-

gen phthalate (KHP, Nacalai Tesque Inc.), and sodium hydroxide (NaOH, Wako Pure Chemical Industries) were used without further purification. Other solvents were also procured from Wako Pure Chemical Industries (Japan), such as n-hexane (C_6H_{14}), ethanol (C_2H_5OH), methanol (CH_3OH), and hydrogen peroxide (H_2O_2, 30%). The coconut oil was purchased from Fujifilm Wako Pure Chemical Corporation, while kenaf oil was extracted from fresh ground seeds using ultrasound-assisted chemical solvent extraction method.

2.2 Oxidation of *p*-MWCNT

The p-MWCNT was first pre-treated using a concentrated acid mixture of 1:1 HNO_3 and HCl using a modified chemical oxidation procedure [26]. Oxidation produced active sites and moieties on the surface of MWCNT, such as carboxylic (−COOH), carbonyl (−C=O), and hydroxyl (−OH) groups [27]. The acid-treated p-MWCNT was referred to as *o*-MWCNT in this study.

2.3 Surface Modification of *o*-MWCNT using 3-APTMS

The surface modification of *o*-MWCNT in $scCO_2$ condition was conducted in a laboratory set-up shown schematically in Figure 1. A 100 mL beaker was initially loaded with 0.3 g of o-MWCNT and 25 mL of 3-APTMS (3 wt%). The mixture was ultrasonicated for 15 min at room temperature. It was subsequently transferred to a 100 mL stainless reactor in which it was heated at 55 °C and pressurized at 9 MPa for 1 h. Gradual depressurization of the system was performed after functionalization, and excess organosilane was collected in vials. The amine-functionalized *o*-MWCNT, represented by NH_2-MWCNT, was dried at 80 °C for 5 h. It was then washed with 100 mL C_2H_5OH, filtered through a funnel, and oven-dried at 80 °C for 2 h.

2.4 Characterization of Catalyst

The TGA was carried out using Perkin Elmer STA 6000 instrument. A specified amount of sample was placed in a ceramic crucible and heated to a temperature of up to 900 °C (heating rate of 20 °C/min) under flowing nitrogen of 50 mL/min. The morphological features and elemental composition of the samples were observed using a Dual Beam Helios Nanolab 600i FESEM-EDX analyzer. It was operated under an accelerating voltage of 2.0 kV, beam current of 86 pA, EDS accelerating voltage of 10.0 kV, and beam current of 0.69 nA. The changes in the crystal structure or orientation of MWCNT samples, before and after surface modification, were examined using Rigaku miniflex 600 analyzer. The surface area (Brunauer-Emmett-Teller), pore-volume, and pore diameter of the samples were determined in Belsorp-mini II (ver.1.2.6) and BELMaster/BELSim (ver.2.3.2). Before measurements, all the samples were outgassed in a vacuum at 433 K and 10^{-4} Pa for 6 h. FTIR spectra were recorded using the attenuated total reflectance accessory technique. Measurements were conducted in the wavenumber range of 4000–600 cm^{-1} and 20 scans. TOF-SIMS (TOF.SIMS 5 by IONTOF) analysis was done to identify the anions and cations present after the addition of 3-APTMS. The following parameters were observed during this analysis: beam of Bi^+, energy of 3000 eV, analysis current of 0.8145 pA, raster mode of random, raster size of 128 pixels × 128 pixels, and time of analysis of 200 seconds. The basic site density of the samples was determined by acid-base back titration method. A sample of 0.02 g of NH_2-MWCNT and 10 mL of 0.02 M of HCl were mixed for 24 h. The catalyst was removed from the mixture by filtration, and 2 mL of filtrate was mixed with 4 mL of 0.02 M NaOH. The liquid solution was neutralized with 0.02 M HCl using phenolphthalein as an indicator.

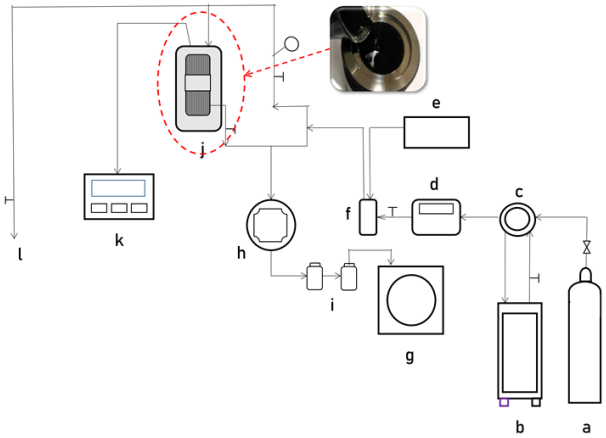

Figure 1. Schematic diagram of supercritical CO_2 system: a. CO_2 gas cylinder, b. chiller (Eyela cool ace ea 1110), c. cooling jacket, d. HPLC pump (Jasco PU 2080), e. cosolvent reservoir, f. mixer, g. CO_2 flowmeter (W-NK type) h. back pressure regulator (Akico), i. collection vials, j. reactor cell (SUS 316; 060333 T-06066) k. temperature controller (AS ONE TR-KN), l. CO_2 discharge port.

2.5 Transesterification of Oil using NH_2-MWCNT as Catalyst

Transesterification reactions were carried out in a 150 mL, three-necked glass-bottom flask equipped with a Graham condenser and a fiber optic thermometer. The flask was loaded with a 12:1 molar ratio of methanol to oil and NH_2-MWCNT catalyst (0.1 g, 10% to oil mass). It was placed in a magnetic stirrer oil bath (AS ONE OBS 200 M) at a reaction temperature of 63 °C and a stirring rate of 600 rpm at 1 h. After reaching room temperature, the mixture was transferred into a vial and added with 15 mL of saturated NaCl solution, 5 mL of n-hexane, and approximately 1 g of Na_2SO_4. The n-hexane was utilized to recover methyl esters from the mixture. Sodium chloride improved the separation of the n-hexane from alcohol layer, while Na_2SO_4 removed H_2O traces. It was placed in a vortex mixer for 5 min and laboratory centrifuge (Tony low-speed centrifuge LCX 100) for 30 min at 5000 rpm.

2.6 Preparation of Standard Fatty Acid Methyl Ester

The standard coconut methyl ester was prepared according to the Association of Official Analytical Chemists (AOAC) 969.33 for fatty acids in oils and fats method [28]. After the separation of FAME from the mixture, a portion of the upper layer was collected and analyzed using Gas chromatography-Mass spectrometer (GC-MS) and a capillary column 19091S-433 HP-5MS (30 mm×0.25 mm, particle size: 2.25 µm). The GC-MS temperature program in this study is similar to a published work found in the references [25]. The coconut oil conversion, as FAME, was determined by comparing the area peaks of dodecanoic acid methyl esters (lauric acid methyl ester) from sample chromatograms. The calculation of % conversion was determined using Equation (1).

$$\%Conversion = \frac{peak\ area\ of\ dodecanoic\ acid\ methyl\ ester_{NH_2-MWCNT}}{peak\ area\ of\ dodecanoic\ acid\ methyl\ ester_{BF_2-NaOH}} \times 100 \quad (1)$$

3. Results and Discussion

3.1 Characterization of Catalyst

3.1.1 Thermogravimetric analysis

Figure 2 compares the thermal stabilities of *p*-MWCNT, *o*-MWCNT, and NH_2-MWCNT. As illustrated, the *p*-MWCNT and o-MWCNT had weight loss from 30 °C to 150 °C due to the removal of remaining moisture from the samples. This same graph further demonstrated the elimination of carboxylic groups from *o*-MWCNT as it reached 150 °C. On the other hand, it can be seen that NH_2-MWCNT had three stages of weight loss at 30, 140, and 360 °C. At a temperature range of 30–140 °C, NH_2-MWCNT had eliminated its moisture and ethanol solvent by up to 8% weight. A slightly moderate weight loss of 4% from 140 °C to 560 °C is associated with the removal of carboxylic and carbonyl functional groups. Finally, the NH_2-MWCNT weight reduction from 560 °C to 900 °C is correlated with the continuous decomposition of chemically bonded organosilane compounds.

3.1.2 Fourier-transform infrared analysis

The FTIR spectrum of NH_2-MWCNT in transmittance mode is shown in Figure 3. At wavelengths between 2625 cm^{-1} and 2950 cm^{-1}, the NH_2-MWCNT spectrum showed changes in

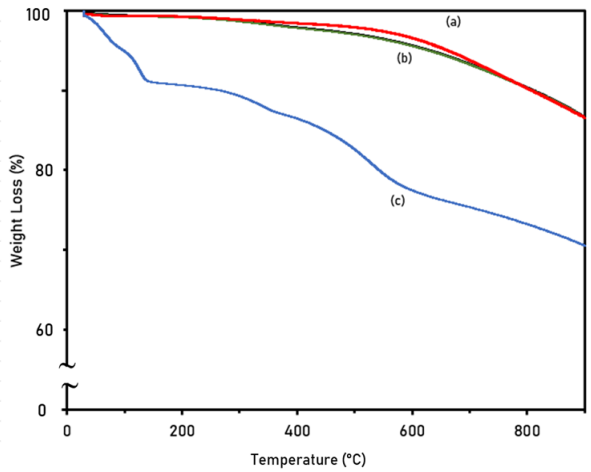

Figure 2. Thermogravimetric profiles of (a) p-MWCNT, (b) o-MWCNT, and (c) NH_2-MWCNT.

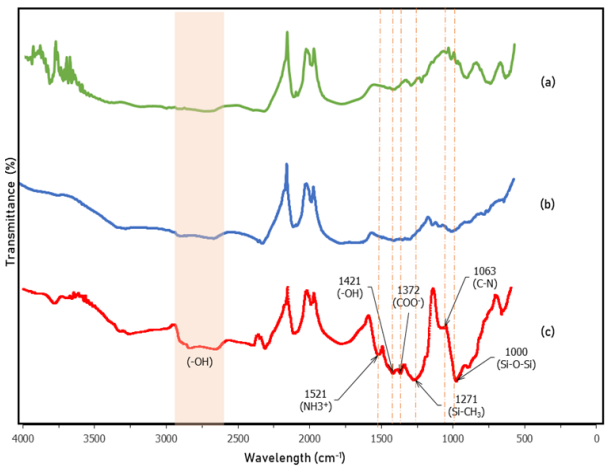

Figure 3. FTIR spectra of (a) p-MWCNT, (b) o-MWCNT, and (c) NH_2-MWCNT.

% Transmittance, which are related with −OH (in carboxylic acids) stretching and −OH (in carboxylic acids) in plane bending, respectively. Also, a prominent peak was observed at 1372 cm^{-1} signifying the presence of the COO^- group. All these observations confirm that MWCNT underwent surface modification by the addition of an acid mixture. The introduction of 3-APTMS, on the other hand, formed new peaks at 1521 cm^{-1} (NH_3^+ deformation) and 1063 cm^{-1} (C−N stretching). Other notable peaks appearing exclusively after organosilane addition include those at 1271 cm^{-1} and 1000 cm^{-1}, matching to Si−CH_3 symmetric deformation and antisymmetric Si−O−Si stretching, respectively. The identified functional groups have established the successful grafting of organosilane using $scCO_2$ on the surface of NH_2-MWCNT.

3.1.3 Field emission scanning electron microscopy – energy dispersive X-ray analysis

The surface morphology of NH_2-MWCNT at 100,000 magnification was observed using FESEM, as appeared in Figure 4. The effects of

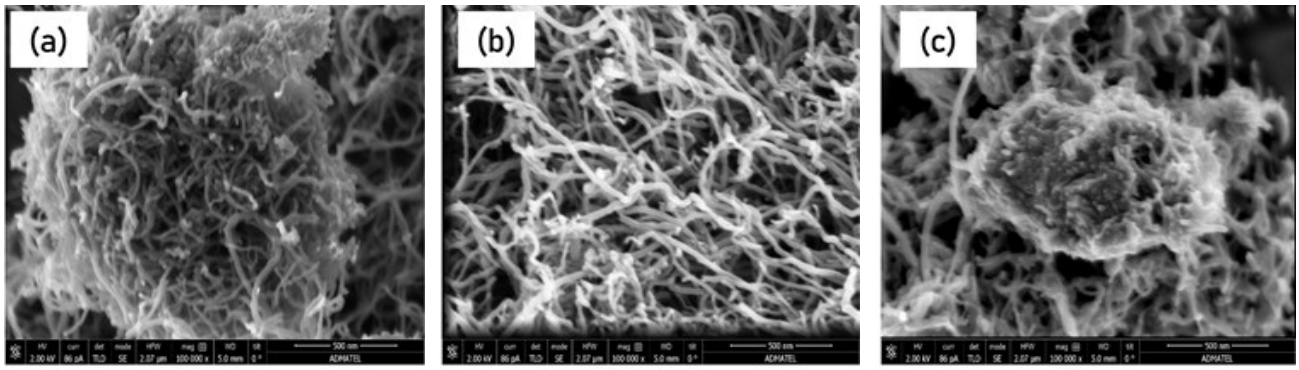

Figure 4. FESEM images of (a) p-MWCNT, (b) o-MWCNT, and (c) NH_2-MWCNT at 100,000 magnifications.

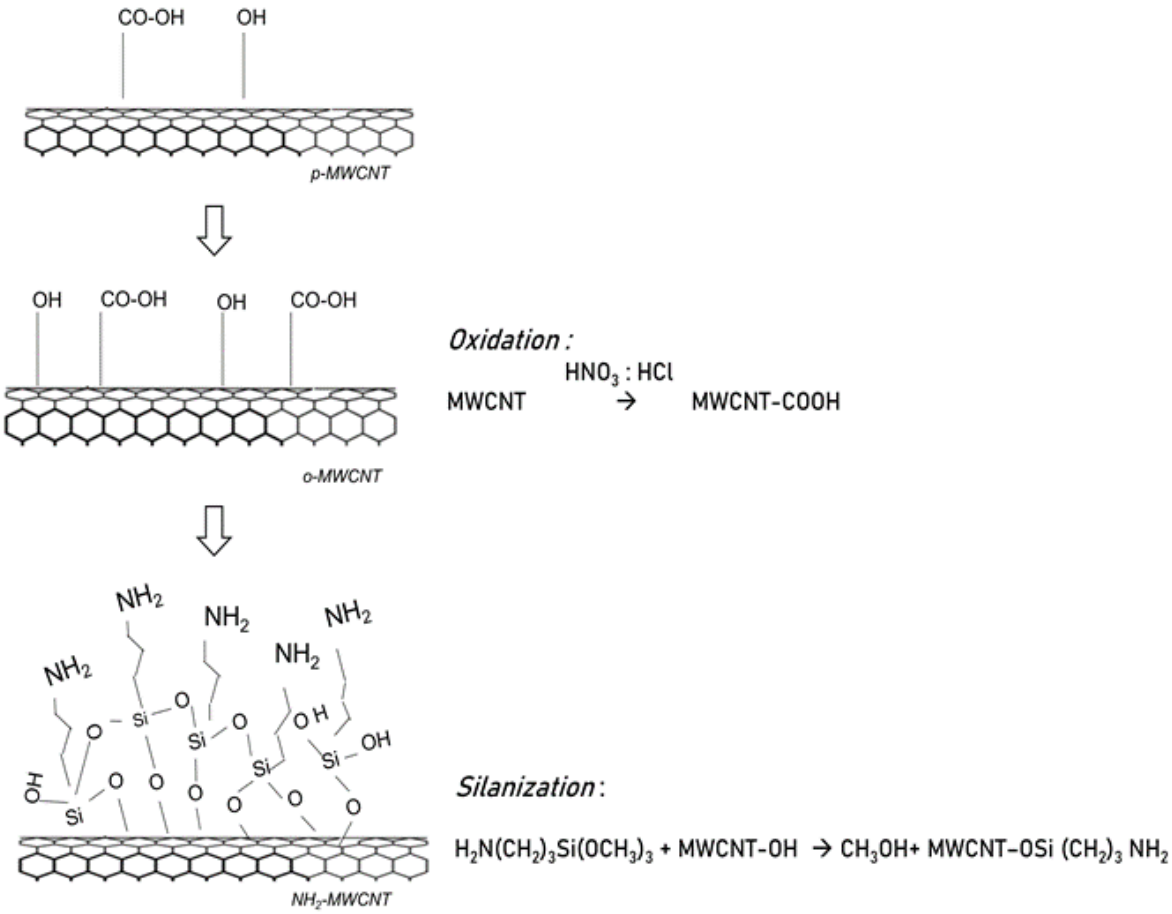

Figure 5. A proposed surface structure of MWCNT during functionalization with 3-APTMS.

Table 1. List of cations in *p*-MWCNT and NH_2-MWCNT using TOF-SIMS analysis.

No.	Ionic Fragment	Mass	Total Ion Intensity		Remarks
			p-MWCNT	NH_2-MWCNT	
1	C^+	12	0.04	0.006	decreased
2	CH^+	13.01	0.01	0.01	same
3	CH_2^+	14.02	0.011	0.02	increased
4	CH_3^+	15.02	0.019	0.02	increased
5	O^+	16	0.001	nd	decreased
6	OH^+	17.001	nd	0.0003	increased
7	NH_3^+	17.025	nd	0.00019	increased
8	NH_4^+	18.039	0.00063	nd	decreased
9	C_2^+	24	0.044	0.001	decreased
10	C_2H^+	25.005	nd	0.002	increased
11	$C_2H_2^+$	26.015	nd	0.019	increased
12	$C_2H_3^+$	27.04	0.055	nd	decreased
13	Si^+	27.974	nd	0.262	increased
14	$C_2H_4^+$	28.04	0.014	0.017	increased
15	SiH^+	28.982	nd	0.086	increased
16	$C_2H_5^+$	29.06	0.032	0.021	decreased
17	$^{30}Si^+$	29.974	nd	0.013	increased
18	$C_2H_6^+$	30.05	0.013	0.007	decreased
19	$^{30}SiH^+$	30.978	nd	0.002	increased
20	$C_3H_2^+$	38.04	0.006	0.007	increased
21	C_3H_3+	39.06	0.038	0.04	increased
22	SiC^+	39.955	nd	0.004	increased
23	C_2O^+	39.99	0.02	nd	decreased
24	$C_3H_4^+$	40.031	nd	0.006	increased
25	$C_3H_5^+$	41.07	0.042	0.036	decreased
26	$C_3H_6^+$	42.08	0.009	0.007	decreased
27	$SiCH_3^+$	43.003	nd	0.022	increased
28	$C_3H_7^+$	43.09	0.028	0.009	decreased
29	CO_2^+	43.997	nd	0.005	increased
30	$C_3H_8^+$	44.09	0.008	nd	decreased
31	$C_4H_2^+$	50.013	nd	0.004	increased
32	$C_4H_3^+$	51.024	nd	0.007	increased
33	$C_4H_5^+$	53.09	0.008	0.008	same
34	$C_4H_6^+$	54.044	nd	0.004	increased
35	$C_4H_7^+$	55.11	0.016	0.0100	decreased
36	$C_4H_9^+$	57.13	0.027	0.01	decreased
37	$C_5H_3^+$	63.021	nd	0.003	increased
38	$C_5H_5^+$	65.042	nd	0.004	increased
39	$C_5H_7^+$	67.061	nd	0.004	increased
40	$C_3H_9N_2^+$	73.079	nd	0.004	increased
41	$C_6H_5^+$	77.035	nd	0.006	increased
42	$C_6H_5N^+$	91.038	nd	0.002	increased
43	$C_8H_{11}O_3^+$	155.07	0.016	nd	decreased
44	$C_{10}H_{19}O^+$	155.15	0.035	nd	decreased

nd - non detected during TOF-SIMS analysis

oxidation (Figure 4(b)) and silanization (Figure 4(c)) on the surface orientation of p-MWCNT (Figure 4(a)) are seen from these micrographs. Oxidation slightly loosened the carbon nanotubes but maintained their long and cylindrical-shaped structure. On the other hand, the addition of 3-APTMS made the MWCNT clustered together in bundles and groups. The organosilane appears to be a uniformly distributed material covering the surfaces and sides of each MWCNT bundle. The surface structure modification on MWCNT, after oxidation and silanization, is illustrated in Figure 5. During the oxidation process, hydroxyl (−OH) and carboxyl (−COOH) groups are introduced, and the −OH from these groups reacts with 3-APTMS during silanization.

3.1.4 Time-of-Flight Secondary Ion Mass Spectrometry Analysis

The lists of positive and negative ions present in p-MWCNT and NH_2-MWCNT were summarized in Tables 1 and 2. Generally, more hydrocarbon cations and anions were identified after oxidation and addition of 3-APTMS. This result suggests the formation of intermediates in an organic reaction under $scCO_2$ conditions.

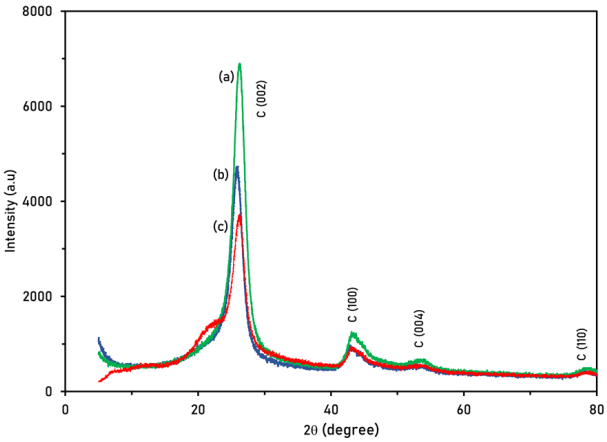

Figure 6. X-ray diffraction pattern of (a) *p*-MWCNT, (b) *o*-MWCNT, (c) NH_2-MWCNT.

Table 2. List of anions in *p*-MWCNT and NH_2-MWCNT using TOF-SIMS analysis.

No.	Ionic Fragment	Mass	Total Ion Intensity		Remarks
			p-MWCNT	NH_2-MWCNT	
1	C^-	12	0.057	0.035	decreased
2	CH^-	13.01	0.026	0.085	increased
3	CH_2^-	14.02	0.002	0.01	increased
4	NH^-	15.01	nd	0.001	increased
5	O^-	16	0.081	0.147	increased
6	OH^-	17	0.018	0.077	increased
7	NH_4^-	17.999	nd	0.00039	increased
8	C_2^-	24	0.416	0.03	decreased
9	C_2H^-	25.01	0.118	0.055	decreased
10	CN^-	26.006	nd	0.064	increased
11	Si^-	27.977	nd	0.004	increased
12	SiH^-	28.986	nd	0.004	increased
13	SiH_2^-	29.993	nd	0.001	increased
14	$^{30}SiH^-$	30.982	nd	0.00361	increased
15	O_2^-	31.98	0.002	0.002	same
16	HS^-	32.98	nd	0.000225	increased
17	Cl^-	34.973	nd	0.009	increased
18	C_3^-	36.006	nd	0.002	increased
19	$^{37}Cl^-$	36.97	nd	0.003	increased
20	C_3H^-	37.014	nd	0.001	increased
21	$C_3H_2^-$	38.018	nd	0.002	increased
22	$C_3H_3^-$	39.023	nd	0.001	increased
23	$C_3H_5^-$	41.012	nd	0.002	increased
24	C_2O^-	40	0.003	0.001	decreased
25	$SiCH_3^-$	43.003	nd	0.000358	increased
26	C_4^-	48	0.014	0.001	decreased
27	C_4H^-	49.01	0.004	0.001	decreased

nd - non detected during TOF-SIMS analysis

Further analysis showed that more Si-containing cations and anions were present on the surface of NH_2-MWCNT (*e.g.*, Si^+, SiH^+, $^{30}Si^+$, $^{30}SiH^+$, SiC^+, $SiCH_3^+$, Si^-, SiH^-, SiH_2^-, $^{30}SiH^-$, and $SiCH_3^-$). The result of TOF-SIMS analysis had confirmed and quantified the existence of 3-APTMS on MWCNT. It also corroborates with the previous findings in TGA, FTIR, and FESEM.

3.1.5 X-ray diffraction analysis

The XRD analysis was performed to identify any modifications made in the crystallographic structure of *p*-MWCNT. In Figure 6, the XRD patterns of *p*-MWCNT, *o*-MWCNT, and NH_2-MWCNT have sharp peaks at angle 2θ of 25.5° (C002), 43° (C100), 53° (C004), and 77° (C110), which are associated with the reflection of graphite [29]. This figure shows a decrease in the XRD profile intensity of the MWCNT samples after oxidation and silanization, indicating that new functional groups were successfully introduced and grafted.

3.1.6 Elemental composition

The presence of 3-APTMS was also confirmed using an EDX analyzer. Figure 7 illustrates the FESEM-EDX micrographs of NH_2-MWCNT and the two selected areas used in describing the organosilane distribution on the surface. It shows that the organosilane is evenly distributed over the MWCNT, having the same wt% N on spectra 1 and 2 (Table 3). On the other hand, elements, such as C, O, Si, Al,

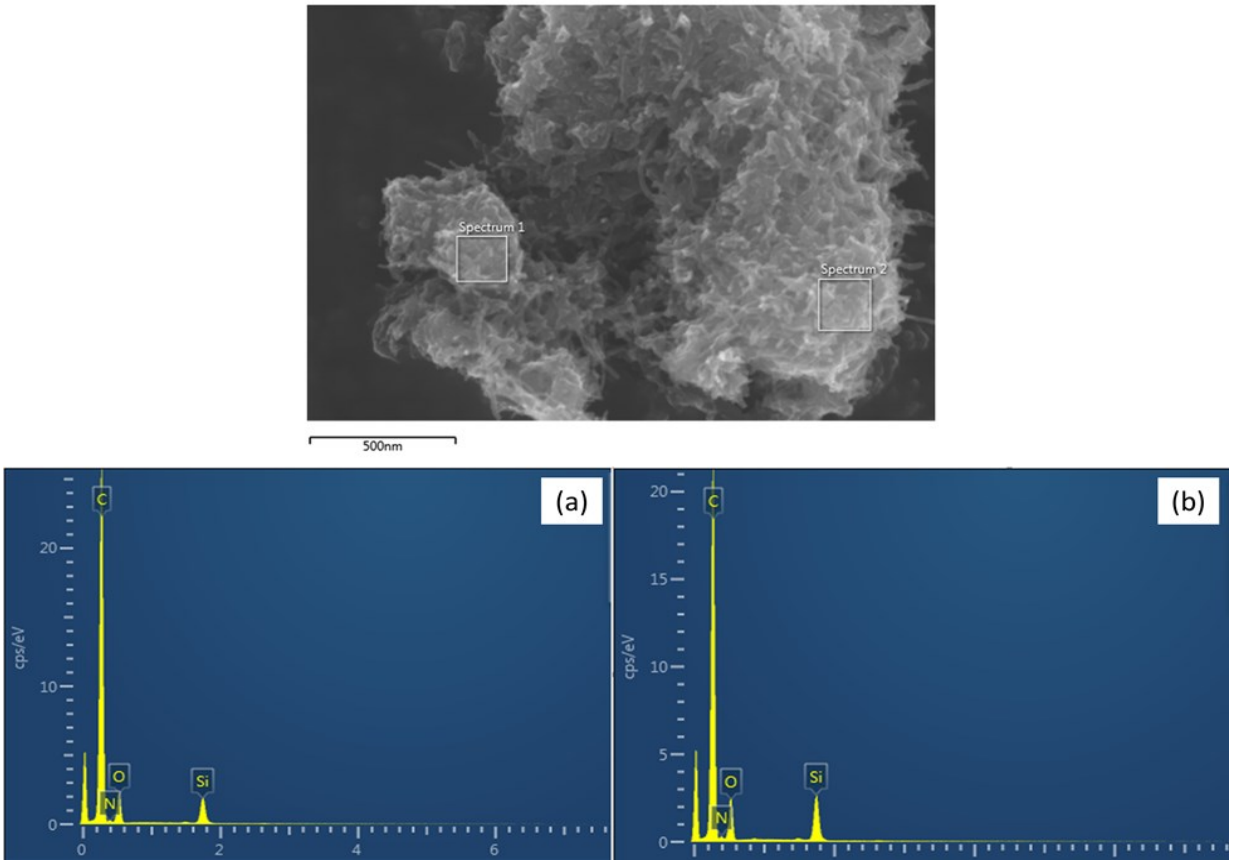

Figure 7. Elemental analysis of NH_2-MWCNT at (a) spectrum 1 and (b) spectrum 2.

Table 3. Elemental composition of MWCNT samples using FESEM-EDX analysis.

Element	Spectra 1 (Area 1)		Spectra 2 (Area 2)	
	p-MWCNT	NH_2-MWCNT	*p*-MWCNT	NH_2-MWCNT
Carbon	92.4	74.4	94.8	78.1
Oxygen	7.5	13.7	4.2	12.4
Silicon	-	7.4	-	5.1
Nitrogen	-	4.4	-	4.4
Aluminum	0.1	`-	-	-
Nickel	-	-	1	-

and Ni, and their corresponding wt% were summarized in Table 3. It is possible that Al and Ni-based compounds were employed in the production of *p*-MWCNT, and they were regarded as impurities of the sample in this study. The absence of these trace metals indicates a successful acid-oxidation treatment and washing of *p*-MWCNT.

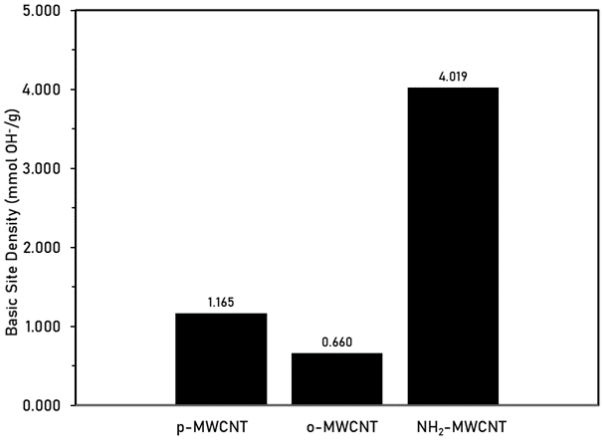

Figure 8. Basic site densities of MWCNT samples. Supercritical CO_2 functionalization conditions: temperature – 55 °C, pressure – 9 MPa, wt% silane – 3 wt%, time – 1 h.

3.1.7 Basic site density

The basic site density of NH_2-MWCNT was measured using the standard acid-base back titration method. As shown in Figure 8, the basic site density increased from 1.165 mmol OH^-/g to 4.498 OH^-/g upon the addition of 3-APTMS. The increase in basic site density is due to the presence of amine groups (–NH_2) from aminosilane that covalently bonded on the hydroxyl groups (–OH) of *o*-MWCNT. As estimated, the basic site density of *o*-MWCNT is much lower than *p*-MWCNT, owing to the presence of acidic functional groups on its surface. This result conforms with elemental analysis, where a higher %N concentration was observed after silanization.

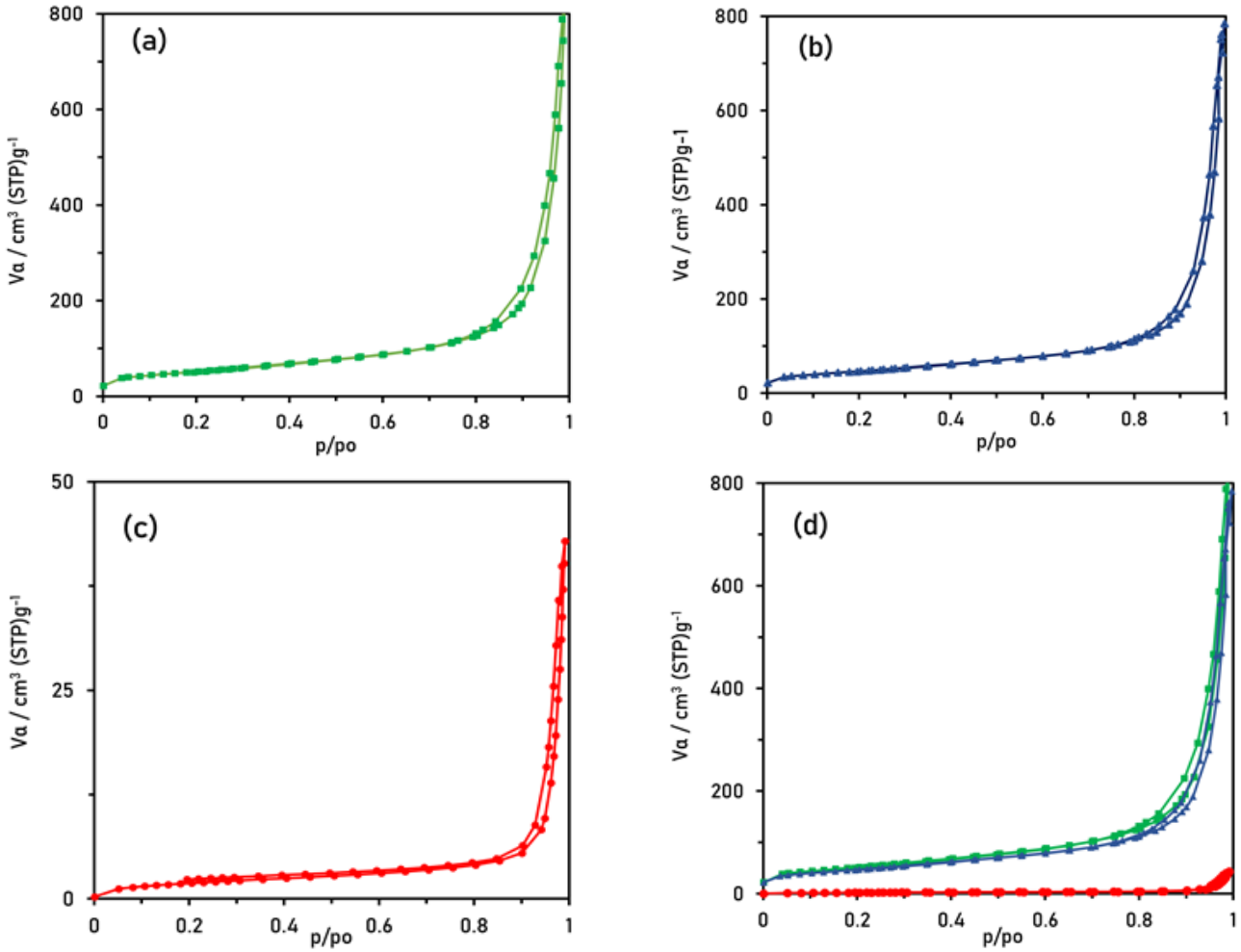

Figure 9. N_2 Adsorption–desorption isotherm of (a) *p*-MWCNT, (b) *o*-MWCNT, (c) NH_2-MWCNT, and (d) *p*-MWCNT, *o*-MWCNT, NH_2-MWCNT.

3.1.8 Brunauer-Emmett-Teller analysis

Figure 9 shows the N_2 adsorption-desorption isotherms of *p*-MWCNT, *o*-MWCNT, and NH_2-MWCNT. All samples exhibited similar isotherms (Type IV) with evident hysteresis loops in the relative pressure about $P/P_o > 0.8$. The presence of a hysteresis loop, over a high range of p/p_o values, indicates capillary condensation taking place at mesoporous particles (pore size = 2–50 nm). Among the three MWCNT samples, p-MWCNT had the highest adsorption capacity due to its highly porous surface, whereas NH_2-MWCNT had the lowest adsorption capacity due to the added amine group on its surface [30]. This was confirmed by the textural and structural properties of MWCNT samples, summarized in Table 4. The oxidation of p-MWCNT caused a reduction in values of its surface area, pore-volume, and pore diameter. Oxidation created defects that cause interference among the nanotubes leading to a smaller surface area and pore diameter [31–33]. In addition, the carboxylic and amine functional groups had slightly taken up the unfilled volume on the pores of MWCNT, thus reducing the pore volumes of *o*-MWCNT and NH_2-MWCNT. In comparing the *o*-MWCNT surface properties to NH_2-MWCNT, the latter's surface area was reduced due to the presence of 3-APTMS, which clusters the nanoparticles in larger particle sizes.

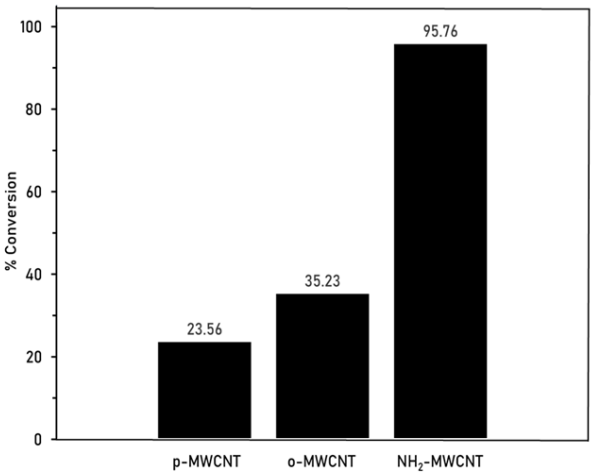

Figure 10. FAME conversion using p-MWCNT, o-MWCNT, and NH_2-MWCNT. Transesterification conditions: feedstock – coconut oil, temperature – 63 °C, wt% catalyst = 10 wt% (3 wt% APTMS), methanol to oil ratio – 12: 1, time – 1 h.

In general, the surface area of catalyst decreased with increased addition of reactive functional groups, such as in other published literature where g- methacryloxypropyltrimethoxysilane was added to silica [34] and metal Sn to silicon dioxide [35]. Furthermore, the addition of organosilane filled up the smaller mesopores of MWCNT, causing an increase in the average pore diameter from 25.90 nm to 39.36 nm and a reduction in pore volume from 1.05 cm^3/g to 0.06 cm^3/g.

3.2 Catalytic Activity

3.2.1 Transesterification of coconut oil

The catalytic activity of MWCNT samples was investigated by transesterification of coconut oil (no detected acid value) at 63 °C, 12:1 methanol to oil molar ratio, 10 wt% catalyst (3 wt% APTMS), and 1 h reaction time. Figure 10 shows the transesterification result, in which *p*-MWCNT and NH_2-MWCNT recorded 23.6% (lowest) and 95.8% (highest) conversion, respectively. The use of *o*-MWCNT as catalyst resulted in a slightly higher conversion of 35.2% compared to *p*-MWCNT. The acidic functional groups of *o*-MWCNT catalyzed the transesterification of coconut oil. On the other hand, the highest % conversion is attributed to the presence of high basic sites in NH_2-MWCNT. The 95.8% conversion is higher than most of the values published in the literature, summarized in Table 5. All solid catalysts from this table were synthesized using toluene as its solvent at a reaction time of approximately 24–48 hours.

The proposed four-step reaction mechanism for amine-catalyzed transesterification of coconut oil is shown in Figure 11. The first step is the reaction of the base catalyst and alcohol, forming protonated NH_2-MWCNT and alkoxide. In this proton reaction transfer, the lone pair electrons on nitrogen form a new covalent bond with the hydrogen atom and produce the conjugate base of alcohol. This process is followed by the reaction of alkoxide and triglycer-

Table 4. BET analysis of NH_2-MWCNT.

Catalyst	Surface Area (m^2)	Total Pore Volume (cm^3/g)	Pore Diameter (nm)
p-MWCNT	179.24	1.25	28.01
o-MWCNT	162.41	1.05	25.90
NH_2-MWCNT	6.43	0.06	39.36

Table 5. Studies on amine-based catalyst for transesterification of triglycerides.

Homogeneous catalysts			
Source of Amine	Feedstock	Result (conversion, %)	Reference
Tetramethylammonium hydroxide (25% solution in methanol)	rapeseed oil	>80	[10]
di-ethylamine + potassium hydroxide tri-ethylamine + potassium hydroxide tert-Butylamine + potassium hydroxide	cottonseed oil	94.1 92.8 91.3	[11]
Heterogeneous catalysts			
Source of Amine (Catalyst Support)	Feedstock	Result (% conversion)	Reference
3-aminopropyltrimethoxysilane (silica gel)	soybean oil	94.5	[20]
3-aminopropyltriethoxysilane (mesoporous silica) 3-chloropropyltriethoxysilane + piperazine (mesoporous silica) 3-chloropropyltriethoxysilane + guanidine (mesoporous silica)	soybean oil	15 12 99	[21]
Dimethyloctadecyl[3-(tri methoxysi-lyl)propyl] ammonium hydroxides (mesoporous SBA-15 silica)	soybean oil	99.7	[39]
1,3-dicyclohexyl-2-octylguanidine (mesoporous SBA-15 silica)	soybean oil	92.6	[6]
3-aminopropyltriethoxysilane (mesoporous template silica) 2,3-aminoethylamino propyltrimethox-ysilane (mesoporous templated silica) 3-diethylaminopropyltrimethoxysilane (mesoporous templated silica)	Tributyrin	8.9 22 26.7	[22]

Table 6. Coconut fatty acid methyl ester.

Retention Time	Fatty Acid Methyl Ester	Chemical Formula	%wt Composition
2.046	Octanoic acid, methyl ester (*Caprylic acid methyl ester)*	$C_9H_{18}O_2$	10.62
3.255	Decanoic acid, methyl ester *(Capric acid methyl ester)*	$C_{11}H_{22}O_2$	8.45
5.672	Dodecanoic acid, methyl ester *(Lauric acid, methyl ester)*	$C_{13}H_{26}O_2$	48.99
9.273	Tetradecanoic acid, methyl ester *(Myristic acid, methyl ester)*	$C_{15}H_{30}O_2$	19.13
13.529	Hexadecanoic acid, methyl ester *(Palmitic acid, methyl ester)*	$C_{17}H_{34}O_2$	7.14
17.326	9-Octadecenoic acid (z)- methyl es-ter *(Oleic acid, methyl ester)*	$C_{19}H_{36}O_2$	3.81
17.882	Octadecanoic acid, methyl ester *(Stearic acid, methyl ester)*	$C_{19}H_{38}O_2$	1.86

ides, forming a tetrahedral intermediate. Then, these tetrahedral intermediates produced the initial methyl ester and diglyceride anion. Finally, the base catalyst was recovered, and another catalytic cycle took place. The methyl esters produced using the NH_2-MWCNT were identified and quantified using GC-MS. The chromatograms and % composition of coconut methyl esters are presented in Figure 12 and Table 6, respectively.

The $scCO_2$ method of functionalization is proven effective in grafting 3-APTMS on o-MWCNT, even in a slightly low-pH environment. This low-pH condition is caused by a reversible reaction of alcohol and CO_2 that produces carbonic acid and a lower pH environment [36]. In this study, the use of $scCO_2$ has reduced the reaction time, solvent waste generation and eliminated the multi-step method of surface modification.

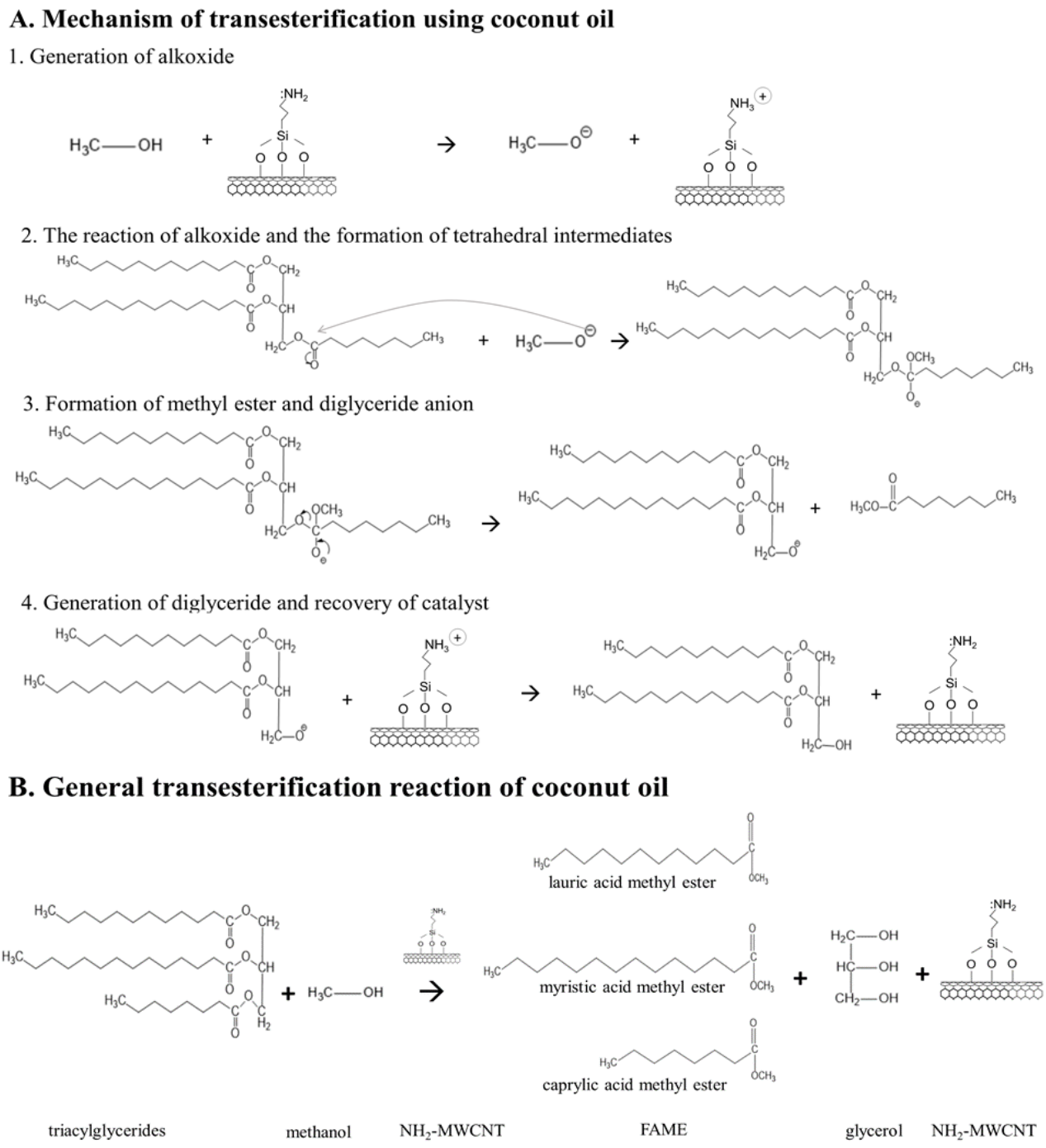

Figure 11. Proposed reaction mechanism for transesterification of coconut oil.

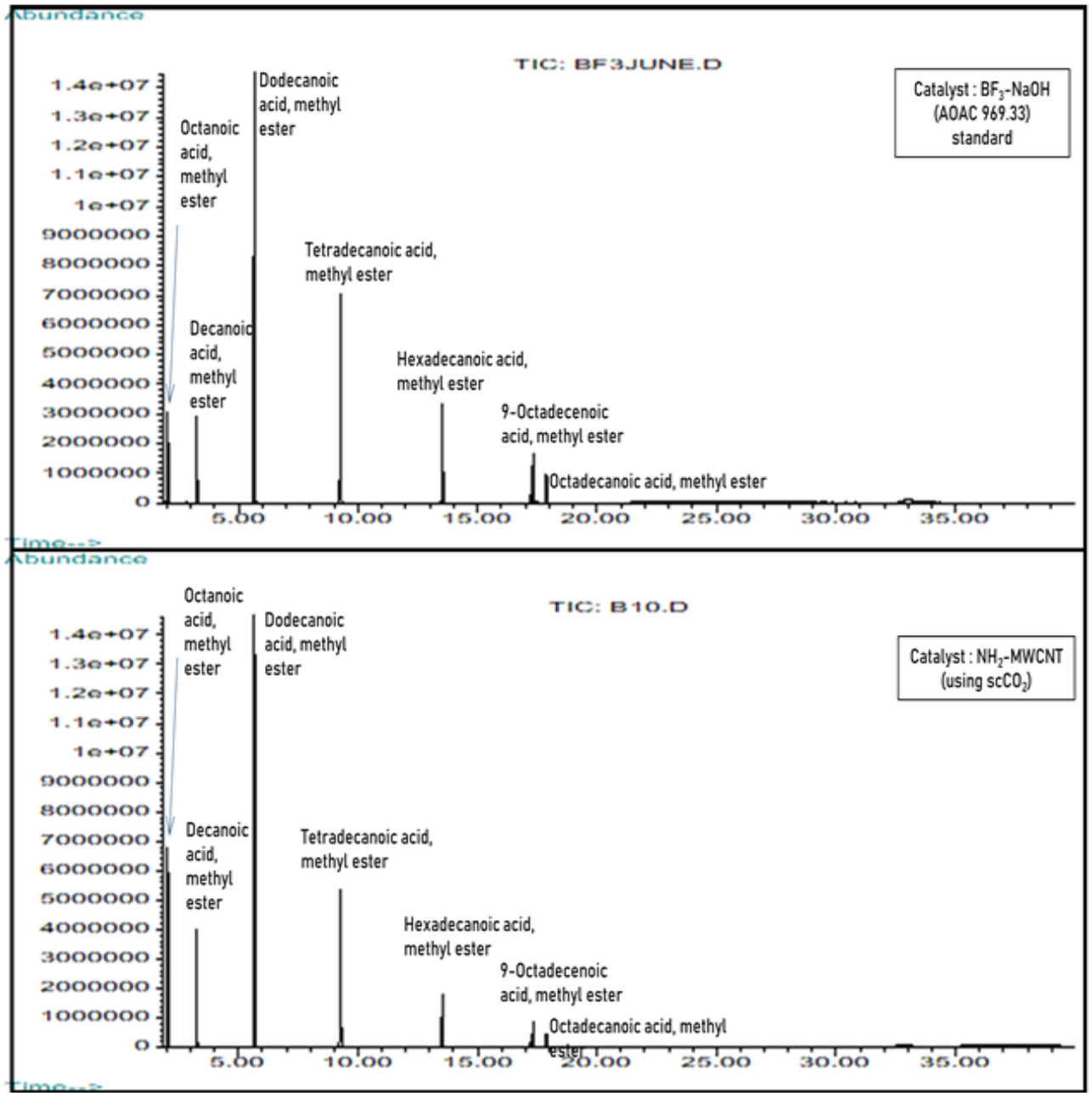

Figure 12. GC-MS chromatogram of coconut methyl ester using NH_2-MWCNT catalyst.

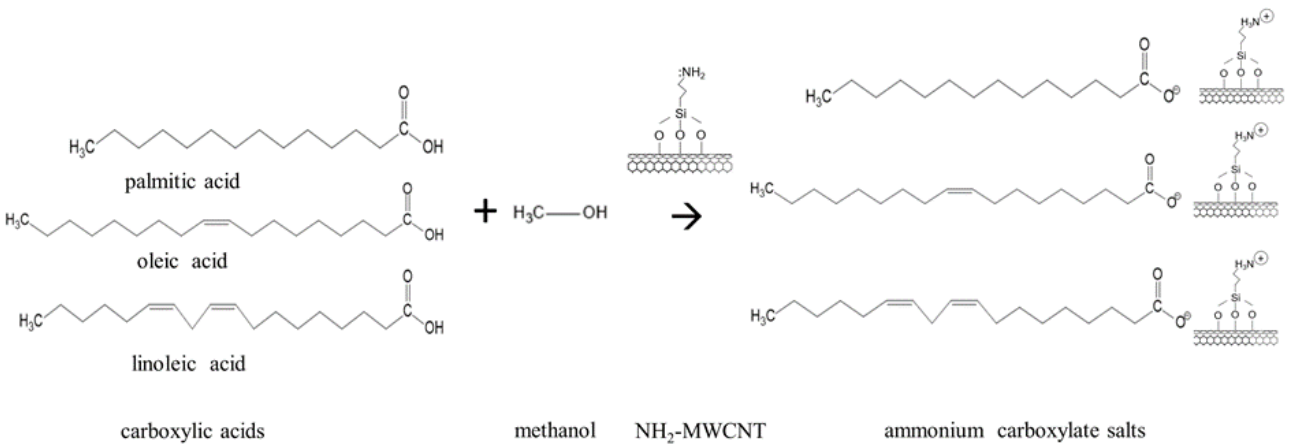

Figure 13. Formation of ammonium carboxylate salts during transesterification of kenaf oil.

3.2.2 Transesterification of Kenaf Oil

The NH_2-MWCNT was also used as a catalyst in the conversion of kenaf oil (acid value = 116.20 mg KOH/g of oil) to biodiesel. After an hour of transesterification, carboxylate salts were formed, and no FAME was found when the sample was injected into GC-MS. The free fatty acids of kenaf oil reacted with amine and resulted in salts formation at 63 °C. Ammonium carboxylate salts are formed when there is an internal acid-base reaction of the amine and carboxylic units [38]. The proposed reaction mechanism of the three highest free fatty acid concentrations in kenaf oil is shown in Figure 13.

3.3 $ScCO_2$ Functionalization Factors and their Effect on Coconut oil Transesterification

The operational parameters affecting the surface modification of NH_2-MWCNT using $scCO_2$, temperature, pressure, and silane concentration, were evaluated using one factor at a time experimentation method. The synthesized catalysts were used in the transesterification of coconut oil, and % conversion was calculated.

3.3.1 Temperature

Three different reaction temperatures of 40 °C, 50 °C, and 60 °C were selected for surface modification of NH_2-MWCNT using 12 MPa and 1.5 wt% silane concentration. As shown in Figure 14, the increasing reaction temperature promotes the grafting of 3-APMTS on the MWCNT surface, resulting in a much higher basic site density. At higher reaction temperatures, the reaction rate and chances of a higher energy collision of the reactants increase. $ScCO_2$ diffusivity may also have increased, resulting in a higher rate of mass transfer between the interfaces of the reactants and attachment of more aminosilane groups on MWCNT surface. This result was also observed in studies involving the use of silane in silica-filled tire tread compounds [39] and crosslinking of Ti-alloy [16], in which the degree of silanization is affected by the reaction temperature. On the same figure, the highest conversion of 69.6% was achieved at 50 °C, which corresponds to an NH_2-MWCNT catalyst having a basic site density of 2.768 mmol OH^-/g. The catalyst having the most number of attached amine groups may not have produced the highest % conversion, a validation that basic site density is only one of several factors affecting a catalyst performance.

3.3.2 Pressure

The effect of pressure on the amount of 3-APTMS grafted on MWCNT is presented in Figure 15. The increase in basic site density was observed from 10 MPa to 12 MPa and slightly decreased as it shifted to 14 MPa. The addition of pressure increased the solvent den-

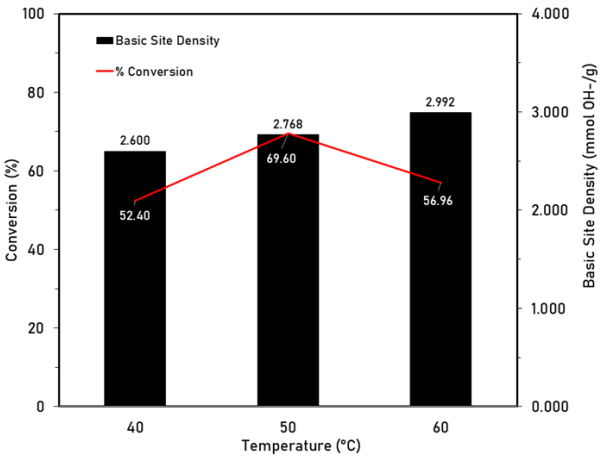

Figure 14. Effect of temperature on basic site density and NH_2-MWCNT catalytic activity. Supercritical CO_2 functionalization conditions: temperature – 40, 50, 60 °C, pressure - 12 MPa, wt% silane – 1.5 wt%, time – 1 h. Transesterification conditions: feedstock – coconut oil, temperature – 63 °C, wt% catalyst – 10 wt% (1.5 wt% APTMS), methanol to oil ratio – 12:1, time – 1 h.

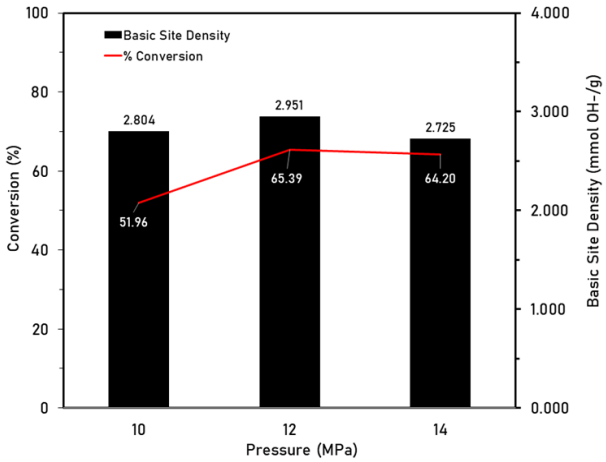

Figure 15. Effect of pressure on basic site density and NH_2-MWCNT catalytic activity. Supercritical CO_2 functionalization conditions: pressure – 10, 12, 14 MPa, temperature – 50 °C, wt% silane – 1.5 wt%, time – 1 h. Transesterification conditions: feedstock – coconut oil, temperature – 63 °C, wt% catalyst – 10 wt% (1.5 wt% APTMS), methanol to oil ratio – 12:1, time – 1 h.

sity and solvent power of $scCO_2$ [40]. This condition allows a higher mass transfer rate of 3-APTMS in ethanolic solution and MWCNT. However, at a pressure range of 12 MPa to 14 MPa, the basic site density decreased from 2.951 mmol OH^-/g to 2.725 mmol OH^-/g. The increase in pressure resulted in CO_2 and alcohol interaction forming a carbonic acid that lowers the pH of a mixture [41,42]. The slight change in the pH may have affected the continuous grafting of aminosilane on MWCNT surface, which naturally occurs in an alkaline mixture. On the same figure, the highest conversion of 65.39 % was achieved at 12 MPa, which corresponds to an NH_2-MWCNT catalyst having a basic site density of 2.951 mmol OH^-/g.

3.3.3 Silane Concentration

To investigate the effect of silane concentration on surface modification of NH_2-MWCNT, three different concentrations (1 wt%, 1.5 wt%, and 2 wt%) were used during $scCO_2$ functionalization of *o*-MWCNT at 50 °C and 12 MPa. The prepared silane concentration is lower than in the previous experiments to observe closely its effect in the transesterification of oil. As illustrated in Figure 16, increasing the silane concentration from 1% to 2% increases the basic site density of NH_2-MWCNT. The highest recorded basic site density is 3.099 mmol OH^-/g upon the addition of 2 wt% 3-APTMS. Moreover, the highest conversion of 70.54% was achieved at the same silane concentration.

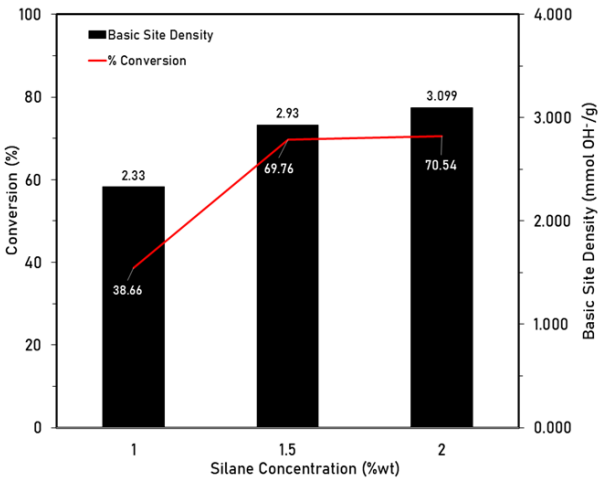

Figure 16. Effect of silane concentration on basic site density and NH_2-MWCNT catalytic activity. Supercritical CO_2 functionalization conditions: wt% silane – 1, 1.5, 2 wt%, temperature – 50 °C, pressure - 12 MPa, time – 1 h. Transesterification conditions: feedstock – coconut oil, temperature – 63 °C, wt% catalyst-10 wt%, methanol to oil ratio – 12:1, time – 1 h.

The relation between two dependent variables- basic site density and % conversion, is shown in Figures 14–16. Based on the experiments conducted, a catalyst with the highest basic site density does not always result in a high biodiesel conversion. The high catalytic performance of NH_2-MWCNT depends on the number of reactive amine groups, surface area, and pore diameter. The catalyst's pore structure is a critical requirement in biodiesel production since a standard triglyceride molecule has a pore diameter of about 5.8 nm. Moreover, a large surface area increases the reaction rate due to a greater chance of reactant particle collision [43].

3.4 Reusability of NH_2-MWCNT

The base catalyst was reused for three cycles in transesterification of coconut oil under the following conditions: 10 wt% catalyst loading (3 wt% of 3-APTMS), 63 °C reaction temperature, 12:1 methanol to oil molar ratio, and 1 h reaction time. Solvents such as methanol and n-hexane are alternately used to wash NH_2-MWCNT and remove unreacted oils, glycerol, and other impurities. It was then dried at 80 °C for 300 min and allowed to cool at room temperature before further use. The summary of the reusability test results of NH_2-MWCNT can be seen in Figure 17.

It shows in the figure the decrease in NH_2-MWCNT catalytic activity after the second (13.5%) and third (20.6%) transesterification reactions. The reduction of % conversion could be attributed to the possible leaching of amine functional groups and blocking of active sites

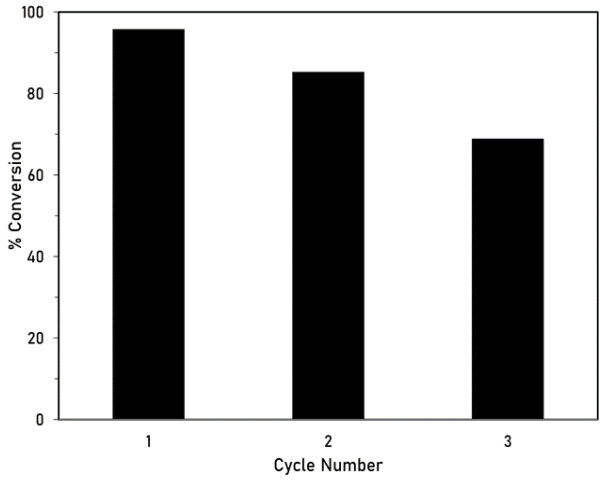

Figure 17. Reusability of NH_2-MWCNT. Transesterification conditions: feedstock – coconut oil, temperature – 63 °C, wt% catalyst = 10% wt (3 wt% APTMS), methanol to oil ratio – 12:1, time – 1 h.

by adsorbed intermediate products, methyl esters, and glycerol on MWCNT. The leaching of amine functional groups can be addressed by increasing the silanization temperature and prolonging the silanization time during the catalyst preparation. It has been proven in other silane-related studies the positive effect of increasing reaction temperature and reaction time [39]. On the other hand, optimizing the transesterification process parameters (*e.g.*, reaction temperature, reaction time, methanol to oil molar ratio, catalyst loading, and mixing speed) will increase catalytic activity at a shorter reaction time, preventing the adsorption of intermediate products into the surface-active sites of NH_2-MWCNT.

4. Conclusions

This study focuses on a heterogeneous base catalyst prepared using supercritical CO_2, and effectively used in the production of coconut methyl esters (>95% conversion). The application of $scCO_2$ resulted in a milder method of catalyst preparation due to the elimination of toxic solvents (*e.g.* toluene), multi-step process, and longer reaction time. This study also reaffirmed that the basic site density of NH_2-MWCNT is just one of the several factors affecting its catalytic activity. The surface area, pore-volume, and pore diameter at different process parameters during $scCO_2$-silanization must be further examined to optimize its catalytic performance. It was proven that the supercritical CO_2 method in grafting amine groups through silanization on multiwalled carbon nanotubes produces an effective catalyst for transesterification of low fatty acid oil.

Acknowledgments

The authors would like to acknowledge the Department of Science and Technology – Philippine Council for Industry, Energy and Emerging Technology (DOST – PCIEERD), Department of Science and Technology- Industrial Technology Development Institute-Advance Device Material Testing Laboratory (DOST – ITDI – ADMATEL), and the e-Asia Joint Research Program (JRP) of Japan-Philippines-Thailand. This work was also partially supported by JST SICORP Grant Number JPMJSC18E2.

References

[1] Mostafa, M., Abdel Aleem, S.H.E., Abdelaziz, A.Y. (2019). Energy Management Solutions for Microgrids. In Rajeev Kumar Chauhan, Kalpana Chauhan (Editors) *Distributed Energy Resources in Microgrids: Integration, Challenges and Optimization*. USA: Academic Press.

[2] Di Serio, M., Tesser, R., Pengmei, L., Santacesaria, E. (2008). Heterogeneous catalysts for biodiesel production. *Energy Fuels*, 22, 207–217. DOI: 10.1021/ef700250g.

[3] de Lima, A.L., Ronconi, C., Mota, C. (2016). Heterogeneous basic catalysts for biodiesel production. *Catalysis Science and Technology*, 6, 1–29. DOI: 10.1039/C5CY01989C.

[4] Quitain, A., Sumigawa, Y., Mission, E., Sasaki, M., Assabumrungat, S., Kida, T. (2018). Graphene oxide and microwave synergism for efficient esterification of fatty acids. *Energy Fuels*, 32, 3599–3607. DOI: 10.1021/acs.energyfuels.8b00119.

[5] Mumtaz, M.W., Adnan, A., Mukhtar, H., Rashid, U., Danish, M. (2017). Biodiesel Production through Chemical and Biochemical Transesterification: Trends, Technicalities, and Future Perspectives. In Mohammad Rasul, Abul kalam Azad, Subhash Sharma (Editors) *Clean energy for Sustainable Development: Comparisons and Contrasts of New approaches*. USA: Academic Press.

[6] Xie, W., Yang, X., Fan, M. (2015). Novel solid base catalyst for biodiesel production: Mesoporous SBA-15 silica immobilized with 1,3-dicyclohexyl-2-octylguanidine. *Renewable Energy*, 80, 230–237. DOI: 10.1016/j.renene.2015.02.014.

[7] Ambat, I., Srivastava, V., Sillanpää, M. (2018). Recent advancement in biodiesel production methodologies using various feedstock: A review. *Renewable & Sustainable Energy Reviews*, 90, 356–369. DOI: 10.1016/j.rser.2018.03.069.

[8] Madhuvilakku, R., Piraman, S. (2013). Biodiesel synthesis by TiO_2-ZnO mixed oxide nanocatalyst catalyzed palm oil transesterification process. *Bioresource Technology*, 150, 55–59. DOI: 10.1016/j.biortech.2013.09.087.

[9] Navas, M., Lick, I., Bolla, P., Casella, M., Ruggera J. (2018). Transesterification of soybean and castor oil with methanol and butanol using heterogeneous basic catalysts to obtain biodiesel. *Chemical Engineering Science*, 187, 444–454. DOI: 10.1016/j.ces.2018.04.068.

[10] Čerče, T., Peter, S., Weidner, E. (2005). Biodiesel-transesterification of biological oils with liquid catalysts: Thermodynamic properties of oil–methanol–amine mixtures. *Industrial & Engineering Chemistry Research*, 44, 9535–9541. DOI: 10.1021/ie050252e.

[11] Yao, J., Ji, L., Sun, P., Zhang, L., Xu, N. (2010). Low boiling point organic amine-catalyzed transesterification of cottonseed oil to biodiesel with trace amount of KOH as co-catalyst. *Fuel*, 89, 3871–3875. DOI: 10.1016/j.fuel.2010.07.003.

[12] Plueddemann, E.P. (1982). *Silane Coupling Agents*. 2nd ed. USA.

[13] Kishor, R., Ghoshal, A.K. (2017). Aqueous aminosilane solution grafted three dimensional mesoporous silica for CO_2/N_2 separation. *Microporous and Mesoporous Materials*, 246, 137–146. DOI: 10.1016/j.micromeso.2017.03.023.

[14] Lai, A., Loehde-Woolard, H., McNeary, W., Burger, J., Pfeffer, R., Weimer, A. (2021). Amine-functionalized fumed silica for CO_2 capture through particle molecular layer deposition. *Chemical Engineering Science*, 245, 116954. DOI: 10.1016/j.ces.2021.116954.

[15] Jeong, U., Kim, Y. (2015). Colorimetric detection of heavy metal ions using aminosilane. *Journal of Industrial and Engineering Chemistry*, 31, 393–396. DOI: 10.1016/j.jiec.2015.07.014.

[16] Rodríguez-Cano, A., Cintas, P., Fernández-Calderón, M., Pacha-Olivenza, M., Crespo, L., Saldaña, L., Vilaboa, N., González-Martín, M., Babiano, R. (2013). Controlled silanization – amination reactions on the Ti 6Al 4V surface for biomedical applications. *Colloids and Surfaces B: Biointerfaces*, 106, 248–257. DOI: 10.1016/j.colsurfb.2013.01.034.

[17] Alex, D., Mathew, A., Sukumaran, R. (2014). Esterases immobilized on aminosilane modified magnetic nanoparticles as a catalyst for biotransformation reactions. *Bioresource Technology*, 167, 547–550. DOI: 10.1016/j.biortech.2014.05.110.

[18] Pourhashem, S., Rashidi, A., Vaezi, M., Bagherzadeh, M. (2017). Excellent corrosion protection performance of epoxy composite coatings filled with amino – silane functionalized graphene oxide. *Surface and Coatings Technology*, 317, 1–9. DOI: 10.1016/j.surfcoat.2017.03.050.

[19] Zhang, X., Heinonen, S., Levänen, E. (2014). Applications of supercritical carbon dioxide in materials processing and synthesis. *RSC Advances*, 105, 61137–61152. DOI: 10.1039/C4RA10662H.

[20] Xie, W., Zhao, L. (2013). Aminopropylsilica as an environmentally friendly and reusable catalyst for biodiesel production from soybean oil. *Fuel*, 103, 1106–1110. DOI: 10.1016/j.fuel.2012.08.031.

[21] de Lima, A.L., Mbengue, A., San Gil, R., Ronconi, C., Mota, C. (2014). Synthesis of amine-functionalized mesoporous silica basic catalysts for biodiesel production. *Catalysis Today*, 226, 210–216. DOI: 10.1016/j.cattod.2014.01.017.

[22] Elimbinzi, E., Nyandoro, S.S., Mubofu, E.B., Osatiashtiani, A., Manayil, J., Isaacs, M., Lee, A., Wilson, K. (2018). Synthesis of amine functionalized mesoporous silicas templated by castor oil for transesterification. *MRS Advances*, 3, 2261–2269. DOI: 10.1557/adv.2018.347.

[23] Škerget, M., Knez, Ž., Knez-Hrnčič, M. (2011). Solubility of solids in sub- and supercritical fluids: A review. *Journal of Chemical & Engineering Data*, 56, 694–719. DOI: 10.1021/acs.jced.7b00778.

[24] Zhang, L., She, Q., Wang, R., Wongchitphimon, S., Chen, Y., Fane, A. (2016). Unique roles of aminosilane in developing anti-fouling thin film composite membranes for pressure retarded osmosis. *Desalination*, 389, 119–128. DOI: 10.1016/j.desal.2015.12.024.

[25] Macawile, M.C., Quitain, A., Kida, T., Tan, R., Auresenia, J. (2020). Green synthesis of sulfonated organosilane functionalized multi-walled carbon nanotubes and its catalytic activity for one-pot conversion of high free fatty acid seed oil to biodiesel. *Journal of Cleaner Production*, 275, 123–146. DOI: 10.1016/j.jclepro.2020.123146.

[26] Yu, H., Jin, Y., Li, Z., Peng, F., Wang, H. (2008). Synthesis and characterization of sulfonated single-walled carbon nanotubes and their performance as solid acid catalyst. *Journal of Solid State Chemistry*, 181, 432–438. DOI: 10.1016/j.jssc.2007.12.017.

[27] Peng, Y., Liu, H. (2006). Effects of oxidation by hydrogen peroxide on the structures of multiwalled carbon nanotubes. *Industrial & Engineering Chemistry Research*, 45, 6483–6488. https://doi.org/10.1021/ie0604627.

[28] AOAC, Association of Official Analytical Chemists. (2000). *AOAC Official Method 969.33 fatty acids in oils and fats*. 17th ed. USA.

[29] Khani, H., Moradi, O. (2013). Influence of surface oxidation on the morphological and crystallographic structure of multi-walled carbon nanotubes via different oxidants. *Journal of Nanostructure in Chemistry*, 3, 1–8. DOI: 10.1186/2193-8865-3-73.

[30] Rahmam, S., Mohamed, N., Suriati, S. (2014). The effect of surface area, pore volume, and pore size distribution on the modified multi-walled carbon nanotubes. *Applied Mechanics and Materials*, 625, 148–151. DOI: 10.4028/www.scientific.net/AMM.625.148.

[31] Hu, Y., Ruckenstein, E. (2004). Pore size distribution of single-walled carbon nanotubes. *Industrial & Engineering Chemistry Research*, 43, 708–711. DOI: 10.1021/ie030757+.

[32] Salam, M.A., Burk, R. (2017). Synthesis and characterization of multi-walled carbon nanotubes modified with octadexylamine and polyethylene glycol. *Arabian Journal of Chemistry*, 10, S921–S927. DOI: 10.1016/j.arabjc.2012.12.028.

[33] Mgheer, T.A., Abdulrazzak, F.H. (2016). Oxidation of multi-walled carbon nanotubes in acidic and basic piranha mixture. *Frontiers in Nanoscience and Nanotechnology*, 2, 155–158. DOI: 10.15761/FNN.1000127.

[34] Jiang, J., Cao, J., Wang, W., Xue, J. (2018). How silanization influences aggregation and moisture sorption behaviours of silanized silica: analysis of porosity and multilayer moisture adsorption. *Royal Society Open Science*, 5, 180206. DOI: 10.1098/rsos.180206.

[35] Hajek, J., Kumar, N., Karhu, H., Cerveny, L., Vayrynen, J., Salmi, T., Murzin, D. (2000). Preparation and properties of bimetallic Ru-Sn sol gel catalysts: influence of catalyst reduction. *Studies in Surface Science and Catalysis*, 143, 757–765. DOI: 10.1016/S0167-2991(00)80719-3.

[36] Lang, S.B., Locascio, T.M., Tunge, J.A. (2014). Activation of alcohols with carbon dioxide: intermolecular allylation of weakly acidic pronucleophiles. *Organic Letters*, 16, 4308–4311. DOI: 10.1021/ol502023d.

[37] Xie, W., Fan, M. (2014). Biodiesel production by transesterification using tetraalkylammonium hydroxides immobilized onto SBA-15 as a solid catalyst. *Chemical Engineering Journal*, 239, 60–67. DOI: 10.1016/j.cej.2013.11.009.

[38] Smith, M. (2020). *Biochemistry: An Organic Chemistry*. USA.

[39] Jin, J., Noordermeer, J., Dierkes, W., Blume, A. (2020). The effect of silanization temperature and time on the marching modulus of silica-filled tire tread compounds. *Polymers*, 12(1), 209. DOI: 10.3390/polym12010209.

[40] Scully, N., O'Sullivan, G., Healy, L., Glennon, J., Dietrich, B., Albert, K. (2007). Preparation of a mercaptopropyl bonded silica intermediate in supercritical carbon dioxide: Synthesis, characterisation and chromatography of a quinine based chiral stationary phase. *Journal of Chromatography A*, 1156, 68–74. DOI: 10.1016/j.chroma.2006.12.037.

[41] West, K., Wheeler, C., McCarney, J., Griffith, K., Bush, D., Liotta, C., Eckert, C. (2001). In situ formation of alkylcarbonic acids with CO_2. *Journal of Physical Chemistry A*, 105, 3947–3948. DOI: 10.1021/jp003846y.

[42] Rubi, R.V., Quitain, A., Agutaya, J.K.C., Doma Jr. B., Soriano, A., Auresenia, J., Kida, T. (2019). Synergy of in-situ formation of carbonic acid and supercritical CO_2-expanded liquids: Application to extraction of andrographolide from *Andrographis paniculata*. *Journal of Supercritical Fluids*, 152, 104546. DOI: 10.1016/j.supflu.2019.104546.

[43] Omar, W., Amin, N. (2011). Biodiesel production from waste cooking oil over alkaline modified zirconia catalyst. *Fuel Processing Technology*, 92, 2397–2405. DOI: 10.1016/j.fuproc.2011.08.009.